Journal of Materials Chemistry A

Accepted Manuscript

ROYAL SOCIETY OF CHEMISTRY

www.rsc.org/materialsA

Journal Name

ARTICLE

Design of interfaces in efficient $Ln_2NiO_{4+\delta}$ (Ln = La, Pr) cathode for SOFCs application

Received 00th January 20xx,
Accepted 00th January 20xx

DOI: 10.1039/x0xx00000x

www.rsc.org/

R. K. Sharma[a, b, c], M. Burriel[d], L. Dessemond[a, b], J.M. Bassat[c], E. Djurado[a, b*]

In this work, a novel architecture of $Ln_2NiO_{4+\delta}$ (LnNO; Ln = La, Pr) cathodes is prepared on $Ce_{0.9}Gd_{0.1}O_{2-\delta}$ (CGO) electrolyte by sequentially using screen-printing (SP) and electrostatic spray deposition (ESD) techniques for the first time. Both LnNO samples crystallize into a single Fmmm orthorhombic layered Ruddlesden-Popper structure. The role of the electrode/air and electrode/electrolyte interfaces has been evaluated by impedance spectroscopy. A drastic reduction in polarization resistance (R_{pol}) from 3.33 to 0.42 Ω cm^2 and from 0.83 to 0.08 Ω cm^2 is obtained at 600 °C for LaNO and PrNO, respectively, when the ESD electrode (with a dense thin, ~ 100 nm, LnNO sub-layer) is topped by a SP current collector. A further R_{pol} reduction down to 0.16 and 0.04 Ω cm^2 is successfully obtained for LaNO and PrNO, respectively, when the LnNO sub-layer is replaced by a thicker (~3 µm) porous CGO/LnNO composite sub-layer. This composite sub-layer is playing a main role on obtaining the best electrochemical properties of nickelates available in the literature, to the best of our knowledge. Moreover, values of polarization resistance for both electrodes are constant at 650 °C for 15 days in air, proving their suitability as SOFC cathodes at this intermediate temperature.

Keywords: SOFC cathode, nickelate, interfaces, ESD, impedance spectroscopy

[a] Univ. Grenoble Alpes, LEPMI, F-38000 Grenoble, France
[b] CNRS, LEPMI, F-38000 Grenoble, France
[c] ICMCB, CNRS, Université Bordeaux, 33608 PESSAC, France
[d] Univ. Grenoble Alpes, CNRS, LMGP, F-38000 Grenoble, France

*Corresponding author, Phone: +33-476826684; Fax: +33-476826777; E-mail: elisabeth.djurado@lepmi.grenoble-inp.fr

1. Introduction

Mixed ionic-electronic conductors (MIEC) with K_2NiF_4-type structure have been intensively studied[1, 2] as promising IT-SOFC cathode materials due to their attractive electrochemical performance.[3-8] It has been reported that the Ruddlesden-Popper-type nickelate compounds such as $Ln_2NiO_{4+\delta}$ (Ln = La, Pr and Nd) show sufficient electronic conductivity due to the metal mixed valence (~ 80 to 100 S cm^{-1}) and good ionic transport properties.[9, 10] Indeed, they can accomodate hyperstoichiometric oxygen in interstitial lattice sites in the rocksalt layers of the structure.[11] In addition, the lanthanide nickelates show a promising electrocatalytic activity for oxygen reduction reaction (ORR).[12] They exhibit high values of surface exchange and diffusion coefficients (k* and D*) compared to perovskites.[12-13] Moreover, they are characterized by low thermal expansion coefficient (TEC) values,[2, 3, 14] that are comparable to the most commonly used electrolytes, such as yttria stabilized zirconia (YSZ) and gadolinia doped ceria (CGO).[15-17] However the polarization resistance (R_{pol}) is still too high and its minimization is required to be used as cathodes for SOFC. Several strategies to improve the electrochemical performance have been explored including the addition of a dense base-layer between the electrolyte and the porous electrode, the control of the microstructure, the introduction of an ionically conducting phase to form a composite electrode and the design of the electrode's architecture. For instance, it is possible to fabricate a layer adjacent to the electrolyte with a smaller particle size to maximize the electrocatalytic activity in this region.[18] This sub-layer can be made denser than the bulk porous electrode with a view to improving the electrolyte/electrode contact and to enhance the oxygen transfer to the electrolyte. Thus, the R_{pol} value for $La_2NiO_{4+\delta}$ was found to decrease from 7.4 to 1.0 Ω cm^2 at 700 °C, as reported by Sayers et al.[19] and it was decreased by ~30% at 600 °C (from 1.2 to 0.85 Ω cm^2) with respect to the best porous cell as reported by Hildenbrand.[20] Another approach is to increase the surface area of the bulk electrode to enhance the number of active surface sites yielding better electrochemical performances.[21] The most promising $Pr_2NiO_{4+\delta}$ electrode, has been reported for a mean particle size of ~ 0.4 μm (R_{pol} value down to 0.08 Ω cm^2 at 600 °C).[22] Moreover, composite cathodes, consisting of a matrix phase cathode (electronic conducting or MIEC) and a second phase electrolyte, are gaining importance not only due to further reduction in the R_{pol} valuem but also to good cathode-electrolyte adhesion properties.[23-25] Composite electrodes preparation via infiltration is one of the most effective methods used to increase the triple phase boundary (TPB) area and to improve the cathode efficiency at lower temperature.[26, 27] Recently Nicollet et al.[27, 28] have studied two different composite cathodes based on $La_2NiO_{4+\delta}$ and $Pr_2NiO_{4+\delta}$ infiltrated into a Gd-doped ceria backbone. Very low R_{pol} values of 0.15 Ω cm^2 for $La_2NiO_{4+\delta}$ and 0.075

Ω cm^2 for $Pr_2NiO_{4+\delta}$ at 600 °C were found in comparison to pure $La_2NiO_{4+\delta}$ (0.93 Ω cm^2 at 600 °C)[29] and $Pr_2NiO_{4+\delta}$ (0.15 Ω cm^2 at 600 °C)[29] cathodes deposited by screen-printing on YSZ electrolyte. On the other hand, the infiltration procedure demands several repeated impregnation-calcination steps which limits its use for industrial applications.[30, 31] Recently, we reported a drastic reduction of the R_{pol} from 3.33 to 0.42 Ω cm^2 at 600 °C when a 3-D coral nanocrystalline $La_2NiO_{4+\delta}$ film (mean particle size ~ 150 nm) with a continuous nanometric dense interfacewas topped by a $La_2NiO_{4+\delta}$ current collector.[32]

In this study, we propose for the first time, an alternative fabrication route for $Ln_2NiO_{4+\delta}$ (LnNO; Ln = La, Pr) electrode on CGO electrolyte, in three steps, as follows: A first thin porous CGO film is deposited by SP and sintered. Then, in a second step, it is covered by a 3-D LnNO porous coral-type microstructure by ESD and sintered. A third LnNO layer is topped by SP as a current collector and sintered. The innovative triple layer architecture of the full LnNO electrode resides on the presence of a CGO: LnNO composite thin porous sub-layer (3-4 μm thick) as a consequence of the penetration of the ESD LnNO film into the first SP CGO sub-layer. This new architecture is used with the objective of decreasing the polarization resistance by improving the electrode/electrolyte contact and enlarging the TPB region. A comparison of the electrochemical properties of the triple layer LnNO electrodes on CGO with two other architectures is performed: a single ESD LnNO layer and a double ESD+SP LnNO layer.

2. Experimental

2.1 Materials and solution preparation

Dense CGO ($Ce_{0.9}Gd_{0.1}O_{2-\delta}$) pellets made by pressing discs (20 mm diameter and 1.2 mm thickness) of commercial powder (Solvay) and subsequently fired at 1400 °C for 4 h were used as electrolyte.

Nickel nitrate hexahydrate [Ni $(NO_3)_2$ $6H_2O$, 99.9%, Aldrich], Lanthanum nitrate hexahydrate [La $(NO_3)_3$ $\cdot 6H_2O$, 99.9%, Alfa Aesar], Praseodymium nitrate hexahydrate [Pr $(NO_3)_3.6$ H_2O, 99.9%, Aldrich] citric acid [$C_6H_8O_7$, 99.9%, Alfa Aesar], and ethanol (CH_3CH_2OH, >99.9%, Prolabo) were used as precursors. ESD precursor solutions of 0.02 M (total cation concentration) were prepared in the mixture of 30 ml of ethanol and water (1:2) by adding the stoichiometric amount of $La(NO_3)_3.6$ H_2O, $Pr(NO_3)_3.6$ H_2O and $Ni(NO_3)_2$ 6 H_2O salts and citric acid (20 mol. % in excess). For the SP layers, the CGO and the LnNO current collector, inks based on KD2921 (Zschimmer and Schwarz) solvent were prepared with commercial CGO powder (Solvay) and with LnNO (Ln = La and Pr) powders obtained by auto-combustion. For this process same precursor solution was used as in ESD process, but prepared in pure EtOH. Then solutions were heated at 150 °C till the completion of auto-combustion process in order to

obtain amorphous powders. These amorphous powders were sintered at 950 °C for 6 h (LaNO) and 1100 °C for 4 h (PrNO) in air, respectively, in order to obtain crystallized and single-phase powders.

2.2 Cathode preparation and characterization

The preparation process of the triple layer cathode can be described in three steps interspersed with heat treatments (**Table 1,** samples 5 and 6). A first CGO base-layer porous film is deposited by SP on CGO electrolyte and sintered at 1200 °C for 4 h in air. Then, it is covered by a LnNO (Ln = La, Pr) porous film using the ESD technique, described elsewhere.[33, 34] The optimized ESD conditions in order to obtain a 3-D coral type microstructure are those previously reported in [31]: deposition time of 180 minutes, substrate temperature of 350 °C, nozzle to substrate distance of 50 mm and flow rate of 1.5 mL/h. This LnNO ESD film partially penetrates into the first CGO porous film leading to a denser CGO-LnNO composite base-layer. The crystallization of this LnNO ESD coating is obtained after a heat treatment of only 2 h at 900 °C for LaNO. In the case of PrNO a heat treatment at 1000 °C for 2 h followed by another one at 1050 °C for 2 h in air is required. No reactivity was observed between LnNO and CGO at these temperatures. The third and final step is the deposition of the LnNO current collecting layer (CCL) by SP, calcined at 1050 °C for 2 h in air. Both sintered electrodes, 30 μm thick, present a good adhesion onto the CGO electrolyte as demonstrated by the tape test. The cathode area is 1.54 cm^2.

Two other LnNO electrodes have been prepared on CGO electrolyte with a single ESD layer (**Table 1**, samples 1 and 2) and a double layer (ESD +SP) configuration (**Table 1**, samples 3 and 4).

Six symmetrical cells were prepared with the single, double and triple layer electrode on both sides of the CGO electrolyte in order to be analyzed by impedance spectroscopy. Electrochemical impedance diagrams were recorded between 500 and 700 °C in air in the frequency range from 0.05 Hz to 100 kHz with an ac signal amplitude of 0.02 V at open circuit potential (OCP) by using a PGSTAT 302N (Eco Chemie). Gold grid (Heraeus, 1024 meshes cm^{-2} woven from 0.06 mm dia. wire) was used as current collector. The data were fitted using equivalent circuits with the Zview® software (Scribner Associates) and were normalized to the electrode area. The crystal structure was determined using powder X-ray diffraction (XRD, Philips X'Pert-MPD system, Cu Kα radiation, λ= 1.54056 Å) in Bragg-Brentano configuration. The XRD patterns were refined using Fullprof software in order to determine the lattice parameters.[35] Surface and cross-sectional morphology of the cathodes was characterized using a scanning electron microscope (ZEISS Ultra 55 instrument with field emission gun, FEG). The particle size of the electrodes was estimated from the SEM images using an image analysis tool (Image J software). The composition analysis was performed by energy-dispersive X-ray spectroscopy (EDX) using acceleration

voltage equal to 20 keV. Oxygen overstoichiometry (δ) of $La_2NiO_{4+\delta}$ and $Pr_2NiO_{4+\delta}$ samples (powder scratched from ESD films) was determined by thermogravimetry measurements (TGA-Q50 instrument) under flowing 5% H_2–Ar gas. Data were collected from 25 to 800 °C at the heating rate of 0.5 °C min^{-1}. Long-term stability measurements were also carried out on the LnNO triple layer cathodes at 650 °C for 15 days in air.

Table 1. Sample identification, composition and deposition technique, surface area and sintering conditions of the prepared cathodes on CGO electrolyte.

Samples (architecture)	Composition (Technique)	Surface area [cm^2]	Sintering in air Temperature / time
Sample 1 (single layer)	LaNO (ESD)	2.00	950 °C / 6 h
Sample 2 (single layer)	PrNO (ESD)	2.00	1100 °C / 4 h
Sample 3 (double layer)	LaNO (ESD) + LaNO (SP)	1.54	950 °C / 6 h + 1050 °C / 2 h + 1100 °C / 0.5 h
Sample 4 (double layer)	PrNO (ESD) + PrNO (SP)	1.54	1100 °C / 4 h 1050 °C / 2 h + 1100 °C / 0.5 h
Sample 5 (triple layer)	CGO (SP) + LaNO (ESD) + LaNO (SP)	1.54	1200 °C / 4h 900 °C / 2 h 1050 °C / 2 h
Sample 6 (triple layer)	CGO (SP) + PrNO (ESD) + PrNO (SP)	1.54	1200 °C / 4h 1000 °C / 2 h +1050 °C / 2 h 1050 °C / 2 h

3. Results and discussion

3.1 Structural characterization of the LnNO films

Fig. 1 shows XRD patterns of the LaNO and PrNO films deposited by ESD and SP on a CGO electrolyte previously recovered by a screen-printed CGO porous layer (samples 5 and 6, **Table 1**). For LaNO film, no impurities or secondary phases have been observed neither for the ESD film after sintering at 900 °C for 2 h, nor for the sample 5, after sintering at 900 °C for 2 h followed by 1050 °C for 2 h in air . All diffraction peaks matched well those of the $La_2NiO_{4+\delta}$ phase (ICDD # 01-074-9394) and those of the $Ce_{0.9}Gd_{0.1}O_{2-\delta}$ phase (ICDD # 04-013-6577) originating from both the substrate and the SP sub-layer. In the case of $Pr_2NiO_{4+\delta}$ prepared by ESD, some traces of Pr_6O_{11} and NiO appear as intermediate phases after sintering at 1000 °C for 2 h along with the CGO phase (ICDD # 04-013-6577) coming from both the substrate and the SP sub-layer. Then, after a successive sintering at 1050 °C for 2 h in air (sample 6), they recombine leading to the pure $Pr_2NiO_{4+\delta}$ phase (ICDD #04-014-1778)). No structural modification was detected when the $Pr_2NiO_{4+\delta}$ CCL film was successively screen-printed onto the ESD layer and sintered again at 1050 °C for 2 h. Both LnNO films crystallize in an orthorhombic unit cell with the Fmmm space group (N° 69). The cell parameters, determined from Fullprof software refinement (**Fig. S1 and S2**), are *a* = 5.457(3) Å, *b* = 5.462(8) Å and *c* = 12.690 (6) Å for $La_2NiO_{4+\delta}$ and *a* = 5.391 (4) Å, *b* = 5.453 (8) Å and *c* = 12.446 (3) Å for $Pr_2NiO_{4+\delta}$, in good agreement with previously reported values.[29]

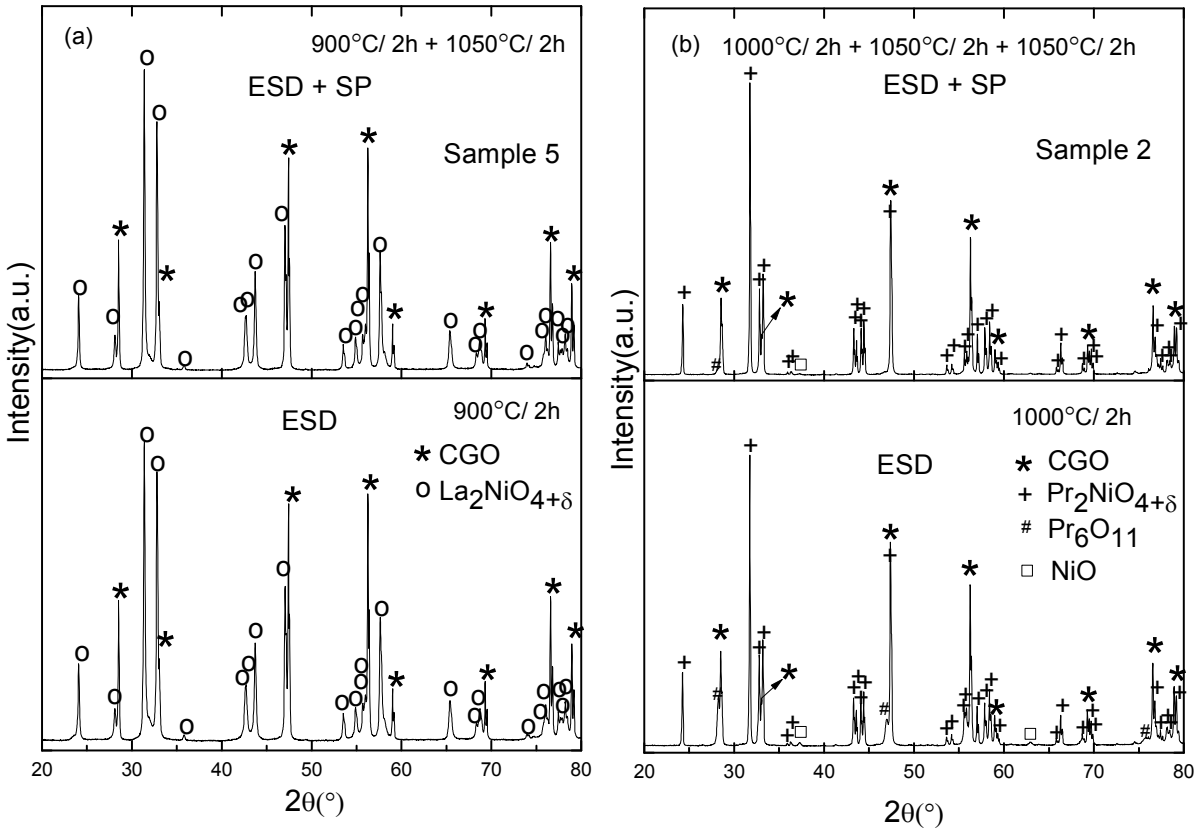

Fig. 1 XRD patterns of the LnNO films coated by ESD and SP on CGO electrolyte previously recovered by a SP CGO sub-layer: (a) $La_2NiO_{4+\delta}$ and (b) $Pr_2NiO_{4+\delta}$.

Moreover, the oxygen overstoichiometry (δ) determined by TGA (**Fig. S3**) was found to be 0.16 and 0.24 for $La_2NiO_{4+\delta}$ and $Pr_2NiO_{4+\delta}$, respectively which is in good agreement with the literature.[29]

3.2 Microstructural characterization of the LnNO films with different architectures

As described in Table 1, one can consider six LnNO electrodes deposited on CGO electrolyte with different architectural designs: *the single layer*: coral-type ESD LnNO layer (sample 1: LaNO and sample 2: PrNO), *the double layer*: ESD + SP LnNO layer (sample 3: LaNO and sample 4: PrNO) and *the triple layer*: characterized by the CGO-LnNO composite base-layer, the ESD LnNO coral-type layer and the SP LnNO current collecting layer (sample 5: LaNO and sample 6: PrNO). In the following, a microstructural study of the LnNO electrode is focused on the construction of the electrode starting by the single, then the double to end with the triple layer architecture. The electrical performance of the triple layer architecture is then investigated and compared to both the single and the double layer electrodes.

Fig. 2 shows SEM surface and cross section images of the samples 1 (LaNO) and 2 (PrNO). Whatever the rare-earth composition (La or Pr), both the samples 1 and 2 are approximately 20 μm thick and show a porous 3-D coral type microstructure, as previously reported by Sharma et al. for LaNO.[32] The ESD process obeys to electrohydrodynamic atomization laws of liquids to produce an aerosol from a liquid precursor which is then directed to a heated substrate. Thus, the microstructure of the resulting film is strongly dependent on the size of the droplets impacting the heated substrate. The droplet size can be controlled through the ESD deposition parameters such as solution flow rate, distance between the substrate and the nozzle and substrate temperature.[36] ESD is a promising and low-cost process which allows a good reproducibility of the coatings. Using similar ESD conditions to the ones reported in our previous article[32] the porous 3-D coral-type microstructure is obtained (substrate temperature of 350 °C, nozzle to substrate distance of 50 mm and flow rate of 1.5 mL/h). This porous microstructure is the consequence of preferential landing of the aerosol droplets on the CGO substrate since nearly dry aerosol droplets impact the substrate.[37] The charges on the substrate surface induced by the strong applied electrostatic field concentrate more where the curvature is greater.[38] So, the charged droplets arriving at the surface will be more attracted towards these more curved areas. This is referred to as ‘‘preferential landing’’. This action is the main route for the particle agglomeration, especially when the droplets are

small and light. Hwang *et al.*[38] have shown that when the substrate roughness increases, preferential landing is promoted leading to particle agglomeration. The average particle size of samples 1 (LaNO) and 2 (PrNO) is estimated to be ~ 150 nm (**Fig. 2b**) and ~ 200 nm (**Fig. 2f**), respectively. The crystal growth is expected to be larger for PrNO in comparison to LaNO since a higher sintering temperature is required to obtain the pure $Pr_2NiO_{4+\delta}$ crystallized phase (1100 °C for 4 h for PrNO compared to 950 °C for 6 h for LaNO). The presence of a thin dense base-layer at the electrolyte-electrode interface, ~ 100 nm thick, can be observed in **Fig. 2d** and **Fig. 2h**, for both sample 1 and sample 2, respectively. As reported previously, [32] this first thin dense interlayer is deposited at the beginning of the ESD process. As a consequence, the first charged liquid droplets containing the precursors solution spread on the polished flat surface of the grounded substrate. The spreading is larger if the precursor solution is characterized by a low evaporation rate. This happens with an EtOH + water (1:2) based precursor solution due to a larger amount of liquid in the charged droplets impacting the substrate. This leads to the formation of a continuous thin dense layer which also facilitates the adhesion of the electrode-electrolyte interface without the need of high sintering temperatures. In order to further improve the flatness and contact between the current collecting grid and the electrode, double layer architecture, samples 3 (LaNO) and 4 (PrNO) were prepared by depositing a screen-printed CCL of similar composition on top of the samples 1 and 2, respectively (**Fig. 3**). The current collecting layer, 20 μm thick, partially penetrates (~ 50 %) the 3-D coral type electrode which further improves the lateral percolation. The average particle size of the screen-printed layer sintered in the same conditions is approximately 450 nm for both compositions. Finally, we have designed another cathodes, samples 5 (LaNO) and 6 (PrNO) by modifying the thin dense sub-layer. It consists of a triple layer electrode obtained by inserting a CGO-LnNO composite base-layer onto the electrolyte (**Table 1**). **Fig. 4** shows the SEM micrographs of sample 6, the ÅÅcross section, the composite base-layer and a schematic of the triple layer design on CGO substrate. Similar morphologies can be observed in sample 5 (**Fig. S4**). A compact base-layer, ~ 3-4 μm thick, is observed. It is the result of the penetration of the electrosprayed LnNO into an initial porous SP LnNO layer forming a base-layer of CGO-LnNO composite, similarly to the infiltration process.[31] The formation of the CGO-LnNO composite of the base-layer was confirmed by EDX in the base-layer region. As an example, EDX signal, collected from an area estimated to 1 μm x 1 μm located in the centre of the sub-layer, is shown in **Fig. 5**.

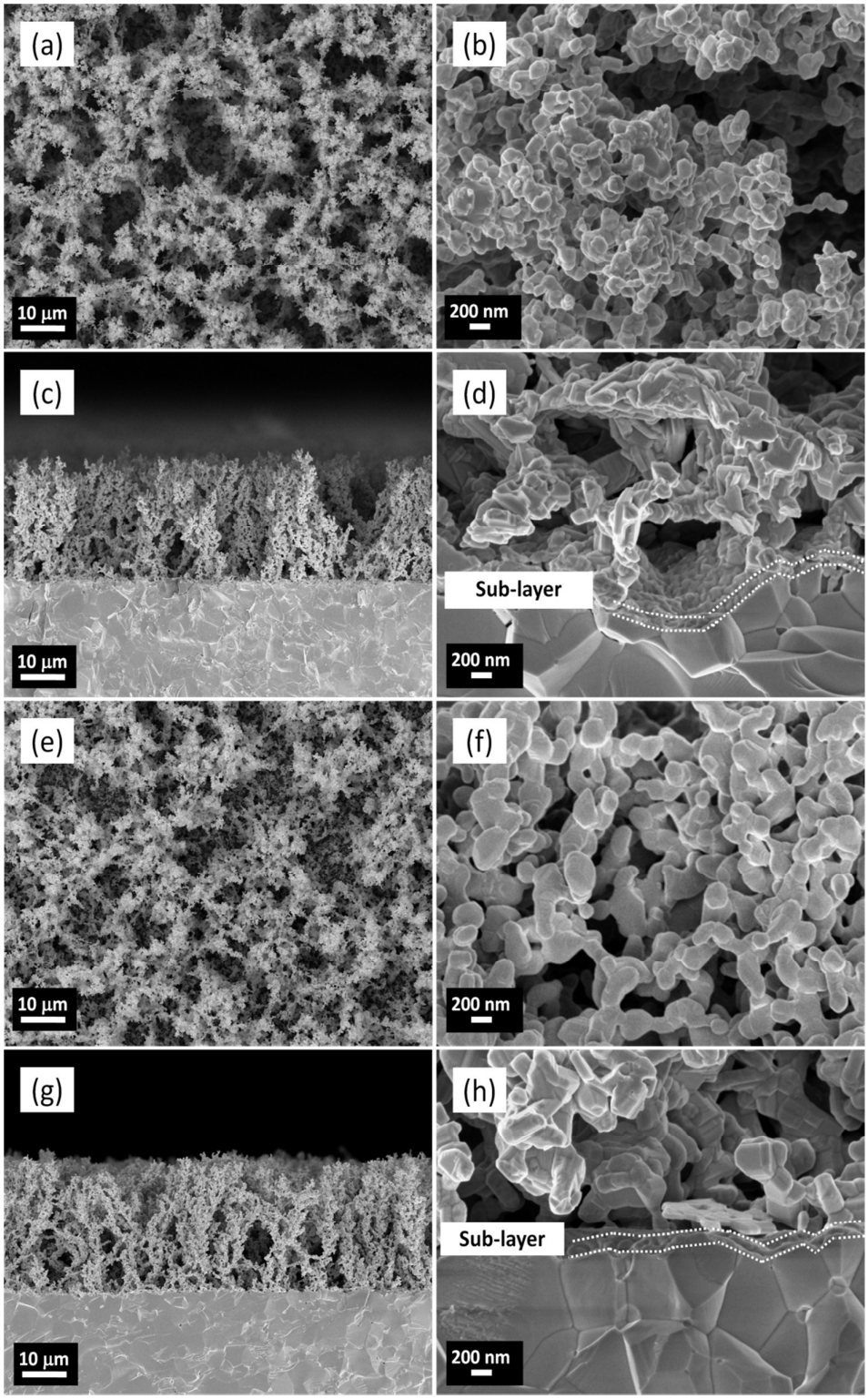

Fig. 2 SEM micrographs of sample 1: (a, b) surface, (c, d) cross section and sample 2: (e, f) surface, (g, h) cross section.

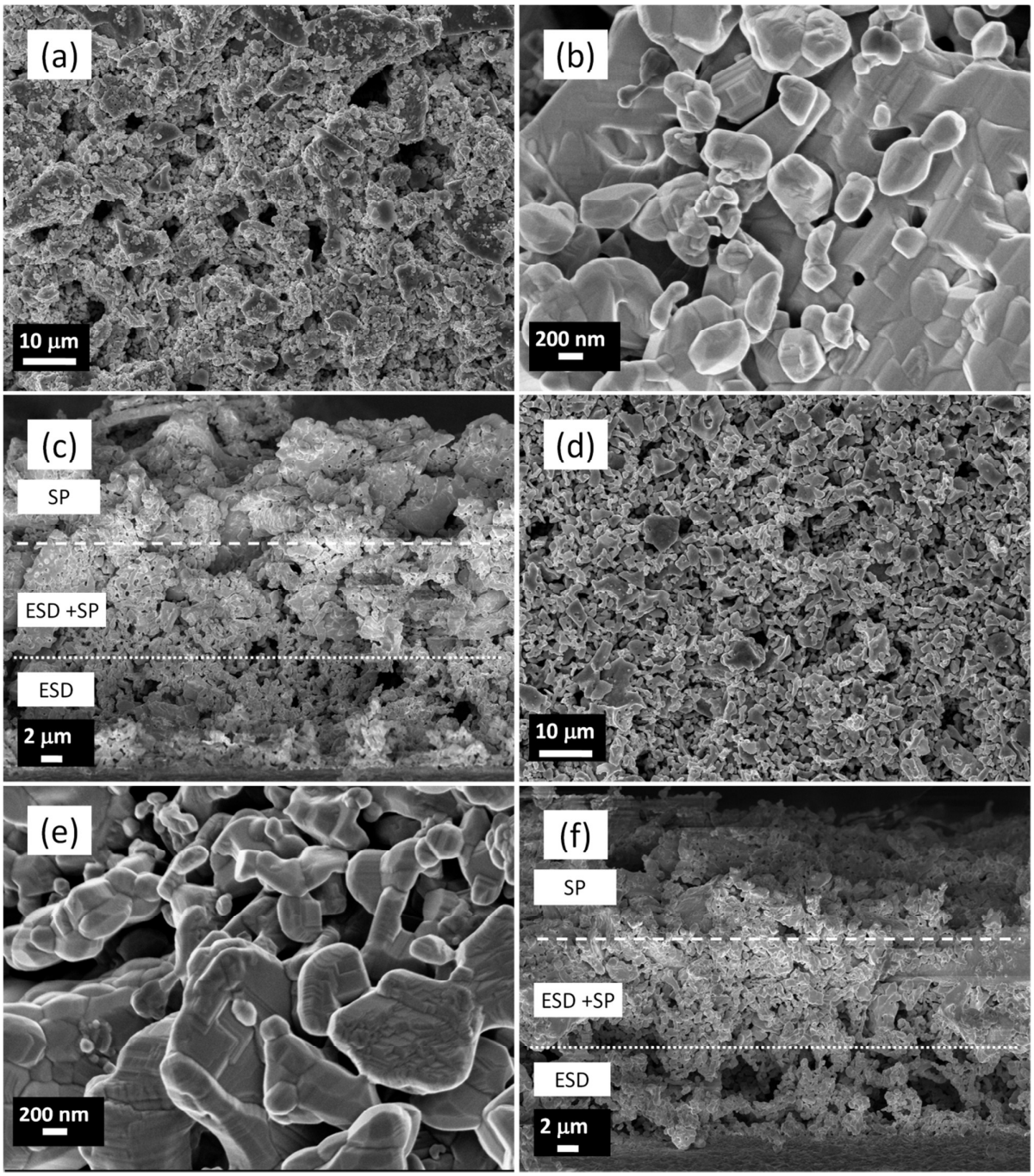

Fig. 3 SEM micrographs of sample 3: (a,b) surface, (c) cross section and sample 4: (d,e) surface, (f) cross section.

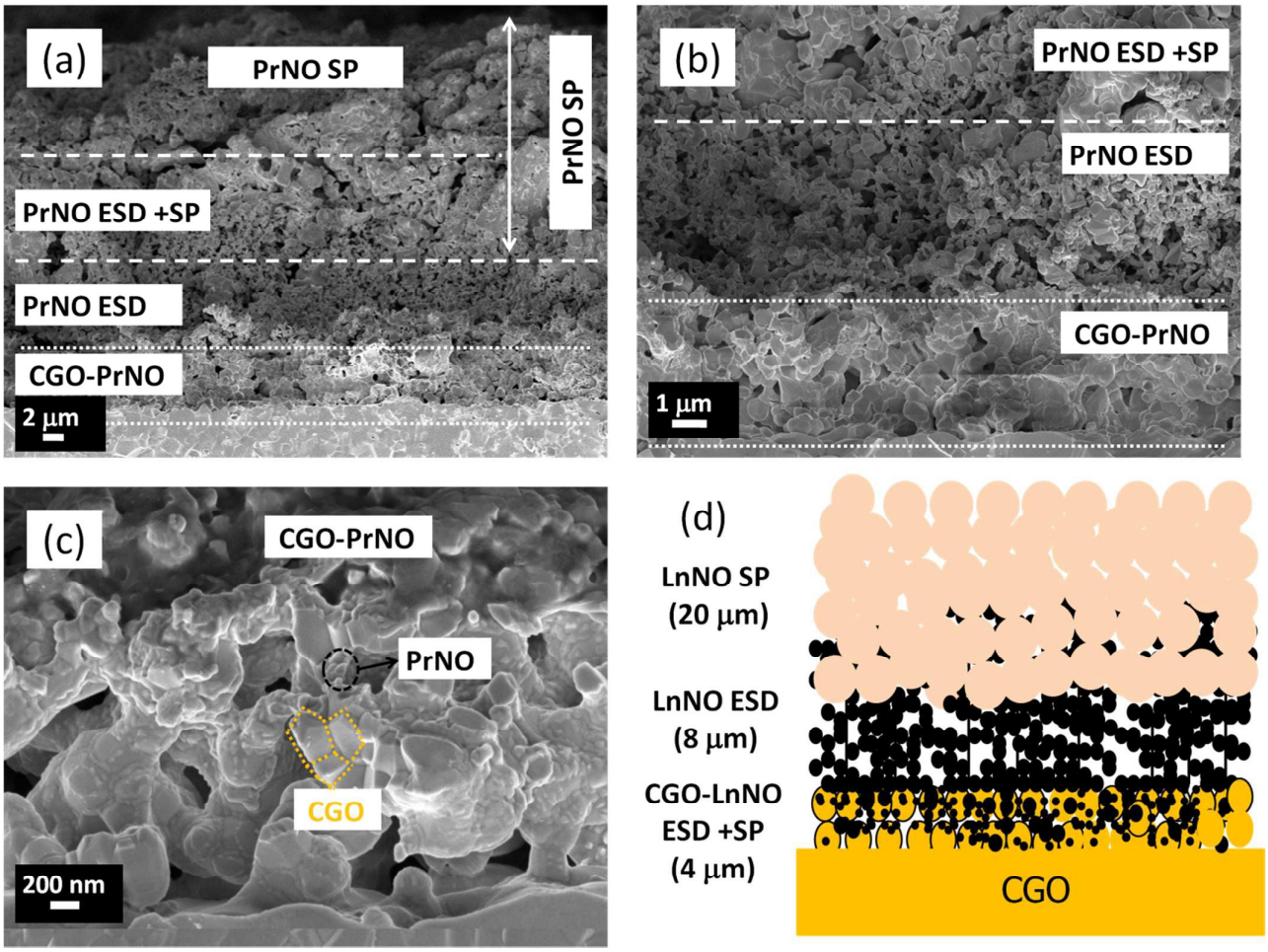

Fig. 4 SEM micrographs of sample 6: (a), (b) cross section, (c) CGO-PrNO sub-layer on CGO electrolyte, (d) schematic of the triple layer design.

The LnNO electrodes with the different designs are characterized by a heterogeneous porosity, larger in the ESD part than the SP one. An estimation of the porosity of the ESD single layer has been performed by comparing the apparent film density with the LnNO theoretical density. The apparent density was obtained by weighing the CGO substrate before and after the LnNO film deposition and measuring the film thickness and diameter. A porosity of approximately 84 vol. % was estimated. This large porosity indicates that plenty of space is available for oxygen molecules to transport especially in the ESD film.

These values are in good agreement with the porosity reported by Sar et al.[39] using FIB-SEM on the CGO/LSCF film also deposited in our group by ESD.

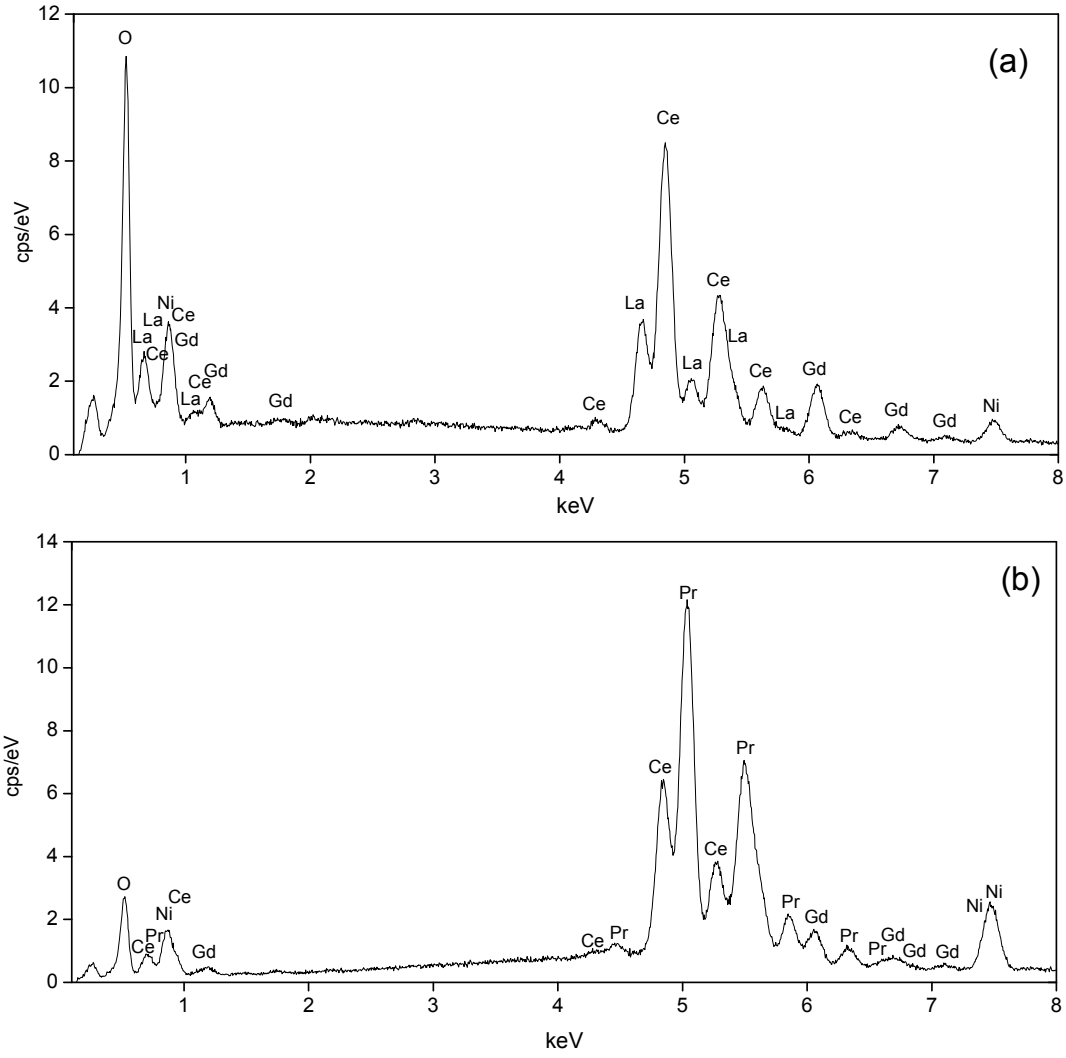

Fig. 5 EDX analysis of the sub-layer region in the LnNO triple layer electrode: (a) sample 5, (b) sample 6.

3.3 Electrochemical properties and stability

The electrochemical properties of the electrodes (samples 1-6, **Table 1**) deposited symmetrically on CGO were investigated by impedance spectroscopy in air at OCV over the temperature range 500 - 700 ºC. In

the following, the electrical properties of the single and the double layer electrode architecture are first presented and then followed by the ones of the triple layer electrode. The impedance diagrams were fitted with an equivalent circuit, as shown in **Fig. 6**, consisting of a combination of several resistances (R)-constant phase element (CPE) parallel circuits, connected in series with an inductance (L) using ZView® software. This electrical element (L), appearing as a high frequency tail below the real axis, represents the contribution of the connecting leads, measuring device and connecting wires to the measured total impedance.[40] The high frequency intercept of the diagrams on the real axis corresponds to the overall ohmic resistance (R_s), including the resistive contributions of the electrolyte, electrode, leads and current collectors. The electrode performance can be quantified by the polarization resistance R_{pol} ($2R_{pol} = 2R_1 + 2R_2 + 2R_3$), which is the difference between the real axis intercepts of the impedance arc. According to the selected analysis, the electrode response is composed by two or three main elementary contributions located at high frequency (1), medium frequency (2) and low frequency (3) depending upon the temperature and composition of the cathodes. The medium frequency arc resistance can be associated with various electrode processes such as adsorption of gaseous oxygen O_2, dissociation of O_2 and charge transfer-diffusion (O^{2-}) in the electrode whereas the high frequency arc is usually attributed to the charge transfer at the electrode/electrolyte interface.[40, 41, 42] The low frequency contribution can be related to a gas impedance due to either porous electrodes or the experimental set-up.[43, 44]

Typical experimental and fitted impedance diagrams, plotted in the Nyquist plane are shown in **Fig. 7a** and **Fig. 7b** for the samples 1 and 3, respectively. Similar data were obtained for the PrNO electrodes (samples 2 and 4). The ohmic resistance (R_s) has been subtracted in order to facilitate comparison between the resistance polarization values (R_{pol}) of the different samples. It is worth mentioning the important effect of the screen-printed CCL layer on the R_s. Adding a SP layer results in a significant decrease of the series resistance regardless of the composition of the electrode. For instance, at 600°C, R_s varies from 14.58 Ω cm² (sample 1) down to 5.43 Ω cm² (sample 2, not shown in **Fig. 7**). Indeed, R_s depends upon the intimate contact at the electrode/electrolyte and current collector/electrode interfaces. Increasing the contact area at both interfaces yields a homogeneous current distribution within the volume of the electrode, i.e. a lower constriction effect of the electrical current lines. As can be seen in **Fig. 2d** and **Fig. 2h** for single layer electrodes, a thin dense layer can be also evidenced at the electrode/electrolyte interface for sample 3 and sample 4. Nevertheless, by using only a gold grid as a current collector (samples 1 and 2), the current lines are not well distributed through the electrode volume. Once the screen-printed layer is added (**Fig. 3**), an homogeneous distribution of current lines within the electrode can be thus anticipated as well as a decrease of the constriction effect of the current lines in the vicinity of the electrode/electrolyte interface. An argument that further supports this

assumption is that the series resistance recorded for both triple layer electrodes is not modified (**Table 2**). Accordingly, any variation of the polarization resistance between the double (samples 3 and 4) and triple layer (samples 5 and 6) electrodes is expected to be related mainly to the electrode morphology.

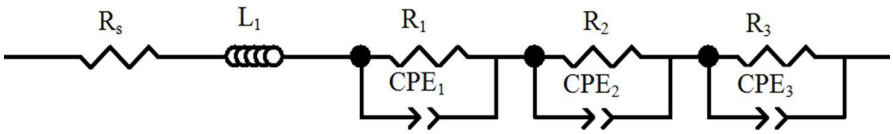

Fig. 6 Equivalent electrical circuit model used for impedance spectra fitting.

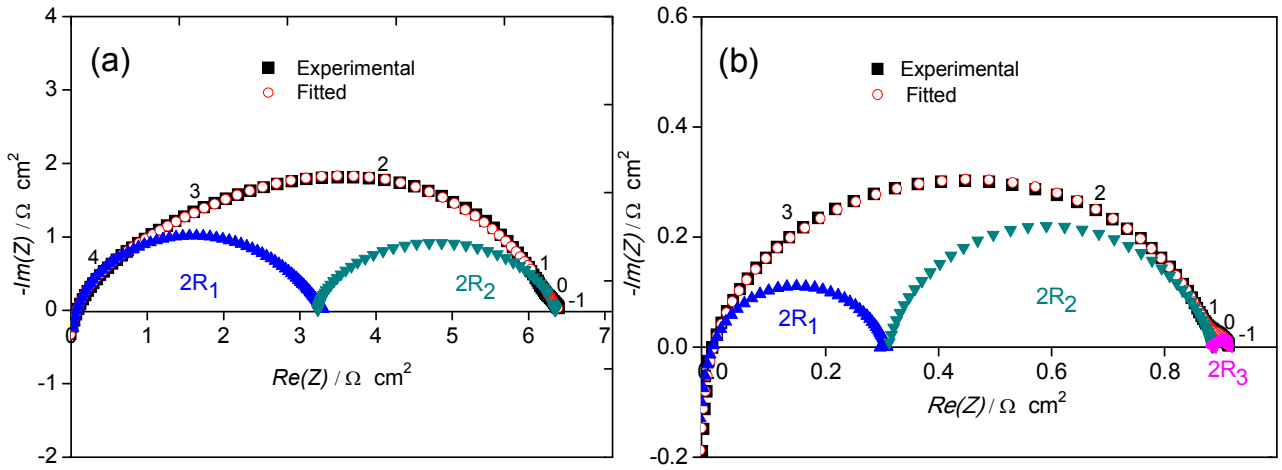

Fig. 7 Nyquist plots recorded at 600 °C in air at OCV: (a) sample 1 and (b) sample 3. The numbers indicate the logarithm of the measuring frequency.

As previously reported[20, 45], the presence of a thin dense layer at the cathode/electrolyte interface (samples 1 and 2) favors the oxygen transfer from the cathode towards the electrolyte and hence leads to better electrode performance. For instance, the polarization resistance was reported to decrease from 0.67 to 0.21 Ω cm^2 and from 1.2 to 0.85 Ω cm^2 at 600 °C for LSCF and LaNO, respectively, when a thin dense layer was deposited by PLD on the TZ3Y electrolyte prior to the screen-printed porous electrode.[20, 45] It is not the case for samples 1 and 2, indeed, the R_{pol} values are found to be 3.33 and 0.83 Ω cm² at 600 °C (Table 2), respectively. These values are found to be higher than the lowest values reported in the literature[51], (2.20 Ω cm², LaNO and 0.28 Ω cm², PrNO) (see Table 3). The coral microstructure of

samples 1 and 2 is highly porous (**Fig. 2a** and **Fig. 2e**) and the contact area with Au grids is too low and thus the whole electrode volume is not totally active for the ORR. Regardless of the electrode microstructure and the related behavior, the oxygen reduction reaction (ORR) from molecular oxygen O_2 into oxygen ions, O^{2-} requires the O_2 supply to the active reaction sites. Consequently, sufficient porosity is needed to facilitate gas permeation and the electronic conductivity must be also maximized at the same time to improve the current collection. This could be the reason for the relatively poor performance of samples 1 and 2. In order to improve the contact between cathode and the grids and hence the effective electronic conductivity of the cathode sheet, the double layer cathodes (samples 3 and 4) were fabricated by depositing a SP layer of the respective composition on the top of the 3-D coral microstructure as a current collector and studied. As for the series resistance, a drastic improvement in R_{pol} is obtained when adding a $La_2NiO_{4+\delta}$ (sample 3) and $Pr_2NiO_{4+\delta}$ SP layer (sample 4), respectively (**Fig. 7**). Double layer cathodes show much better performance: 0.42 Ω cm² at 600 °C (sample 3) and 0.08 Ω cm² at 600 °C (sample 4), respectively. At 600 °C the R_{pol} decreases by a factor of 8 for sample 3 and factor of 10 for sample 4. This is also in good agreement with the improvement in R_s values.

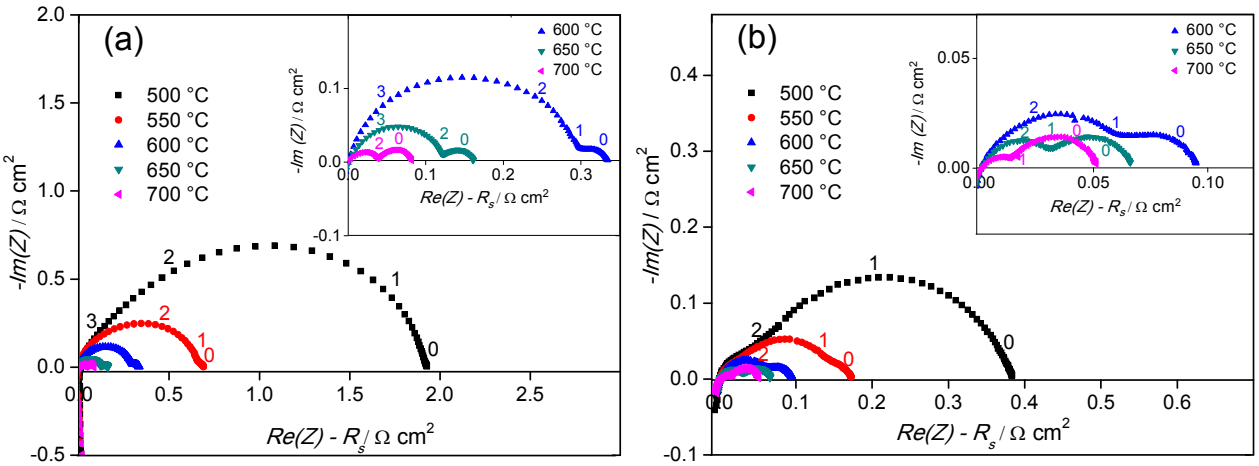

Fig. 8 Nyquist Plots recorded as a function of the temperature (from 500 to 700 ºC) at OCV; (a) sample 5 and (b) sample 6. Inset picture is a zoom-in of the high temperature plot. The numbers indicate the logarithm of the measuring frequency.

This drastic improvement of electrode performance (table 2) of sample 4 over sample 3 (or sample 2 over sample 1) is also due to better mixed ionic-electronic conductivity as well as diffusion properties of PrNO in comparison to LaNO for similar architecture. Indeed these properties are dependent upon oxygen nonstoichiometry (δ); the higher the δ, larger the ionic conductivity and diffusion. From TGA (**Fig. S3**), PrNO shows larger oxygen nonstoichiometry (δ = 0.24) in comparison to LaNO (δ =0.16) in good agreement with the literature.[29]As shown in **Fig. 7**, the frequency distribution of the electrode impedance is not modified by adding the CCL, indicating that the ORR remains the same. In order to further reduce the R_{pol} values, a composite sub-layer was added for samples 5 and 6 (**Fig. 4**). For a given electrode composition the frequency distribution of the electrode impedance is not strongly modified (**Fig. 8**). The ORR is likely to remain similar. On the other hand, the shape of the electrode characteristic is modified since a third elementary contribution (labeled as 3) is clearly observed for temperatures higher than 550 °C (**Table 2**). The fitted and experimental spectra at 600 °C from the inset of **Fig. 8b,** is shown in **Fig. S5.** In order to assess the robustness of the fittings, capacitances and exponents of CPE for all 6 architectures are further given in **Table S1.** It must be emphasized that the R_{pol} value decreases further down to 0.04 Ω cm^2 for sample 5 (LaNO) and to 0.02 Ω cm^2 for sample 6 (PrNO) at 700 °C, respectively. Once again such improvement in sample 6 over sample 5 is due to the better mixed ionic-electronic conductivity and diffusion property of PrNO since architecture is similar (Fig. 4, Fig. S4). Remarkably, the obtained R_{pol} values are lower than those reported in the literature for LnNO based cathodes (**Table 3)**. When a compact composite layer of CGO and LnNO is inserted between the electrolyte and the double layer cathode), a significant decrease in both the high and medium frequency resistances (R_1 and R_2) is observed. Since the series resistances do not vary between double and triple layer electrodes for temperatures higher than 500 °C (**Table 2**), it can be assumed that the constriction effect at the electrode/electrolyte interface is minimized in the chosen temperature range. By considering that the SP layer acts as an optimized current collector for both types of electrodes, and that the microstructure of the ESD and SP layers remains unchanged (**Figures 3 and 4**), one could infer that the polarization resistance remains the same. Nevertheless, adding CGO enhances the ionic conductivity adjacent to the electrolyte and a better contact between CGO and LnNO can be anticipated.[20, 23] The improvement of the electrode performance is likely to be mainly related to the increase of the active electrode thickness by inserting a composite layer. These results are in good agreement with the work previously reported by Nicollet et al.[27, 28] for the composite electrodes, LaNO and PrNO infiltrated into a Gd-doped ceria backbone. Low R_{pol} values of 0.15 Ω cm^2 for LaNO and 0.08 Ω cm^2 for PrNO at 600 °C were reported. Thus the proposed cathodes in this work could be considered as a potential cathode material for IT-SOFC.

As could be expected, R_1 and R_2 decrease by increasing the temperature (**Table 2**). The R_2 values are always larger than those of R_1 (at least a factor of 2 between 500 and 700 °C) suggesting that the oxygen desorption or adsorption process is the rate-limiting step for the ORR.[46-48] As shown in **Table 2**, the magnitude of the (R_3) low frequency contribution (~1 Hz) almost does not vary with temperature. Moreover this contribution is characterized by high capacitance values, C ≈ 2.6 F.cm^{-2} for the LaNO and ≈ 3.3 F.cm^{-2} for the PrNO cathode, respectively. Such contribution has been attributed to the O_2 gas diffusion process through the porous electrode.[49, 50]

Table 2 Comparison of R_s, R_{pol}, R_1, R_2, R_3 values (Ω cm^2) of the three architectures for LaNO and PrNO electrodes (estimated error is < 5 %).

Temperature [°C]	LaNO cathodes														
	Single layer (sample 1)					Double layer (sample 3)					Triple layer (sample 5)				
	R_s	R_{pol}	R_1	R_2	R_3	R_s	R_{pol}	R_1	R_2	R_3	R_s	R_{pol}	R_1	R_2	R_3
500	22.78	13.38	3.86	9.52	---	8.25	2.85	0.82	2.03	---	7.61	0.97	0.29	0.68	---
550	18.96	7.00	2.24	4.76	---	6.40	1.01	0.38	0.63	---	6.35	0.35	0.11	0.23	0.01
600	14.56	3.32	1.63	1.69	---	5.43	0.42	0.11	0.30	0.01	5.28	0.16	0.04	0.11	0.01
	PrNO cathodes														
	Single layer (sample 2)					Double layer (sample 4)					Triple layer (sample 6)				
	R_s	R_{pol}	R_1	R_2	R_3	R_s	R_{pol}	R_1	R_2	R_3	R_s	R_{pol}	R_1	R_2	R_3
500	14.28	2.38	0.91	1.47	---	6.30	0.32	0.12	0.20	---	7.26	0.23	0.10	0.13	---
550	10.74	1.30	0.56	0.74	---	4.76	0.14	0.06	0.08	---	5.50	0.08	0.03	0.04	0.01
600	8.32	0.83	0.18	0.65	---	4.35	0.08	---	0.07	0.01	4.59	0.04	---	0.03	0.01

Table 3 Comparison of minimum R_{pol} value obtained in this study with values reported in the literature for LnNO (Ln= La, Pr) cathode.

Cathode	Electrolyte	R_{pol} [Ω cm^2]	T [°C]	Reference
LaNO infiltrated CGO	CGO	0.15	600	Nicollet et al.[27]
PrNO infiltrated CGO	CGO	0.07	600	Nicollet et al.[28]
LaNO	CGO	2.20	600	Philippeau et al.[51]
PrNO	CGO	0.28	600	
LaNO	YSZ	0.93	600	Vibhu et al.[29]
PrNO	YSZ	0.15	600	
Triple layer LaNO	CGO	0.16	600	Present work
Triple layer PrNO	CGO	0.04	600	

The activation energies deduced from the Arrhenius plots of the polarization resistance R_{pol} (**Fig. 9**) are in good agreement with the values reported in literature.[19, 20, 27] To the best of our knowledge, the R_{pol} value obtained (as low as 0.04 Ω cm² at 700 °C for sample 5 and as low as 0.02 Ω cm² at 700 °C for sample 6) is far better than the minimum R_{pol} values previously reported for pure $La_2NiO_{4+\delta}$ and $Pr_2NiO_{4+\delta}$ based cathodes, as shown in **Table 3**. Moreover, all the results have been found to be reproducible. Such excellent performance of triple layer cathodes indicates that an architectural design of LnNO (Ln = La, Pr) cathodes plays a major role in improving their performance by enhancing the electrode to electrolyte charge transfer as well as the ORR.

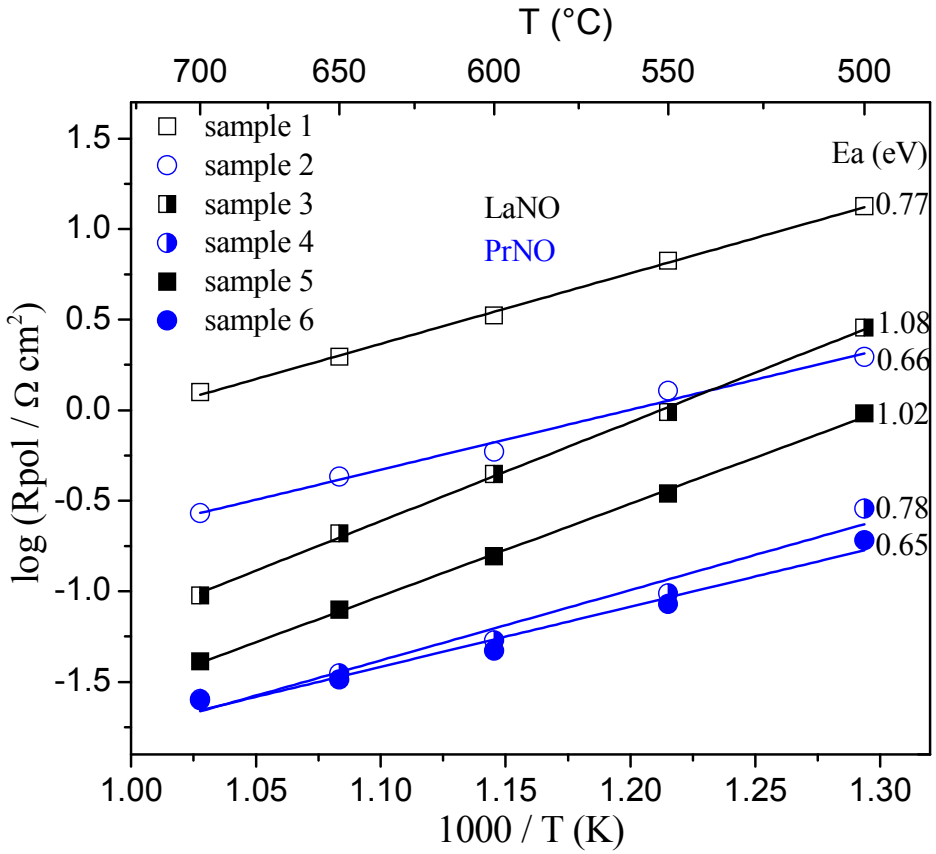

Fig. 9 Arrhenius plot of the R_{pol} in air for six electrodes (OCV conditions) on CGO electrolyte.

Finally, the polarization resistance stability was evaluated for two electrodes (samples 5 and 6) for 360 h at 650 °C and neither of the cathodes shows any significant variation in the polarization resistance at OCV, as shown in **Fig. 10**. Further studies are in progress to evaluate the stability of these nanostructured electrodes after long-term operation under polarization and to test the performance in fuel cells.

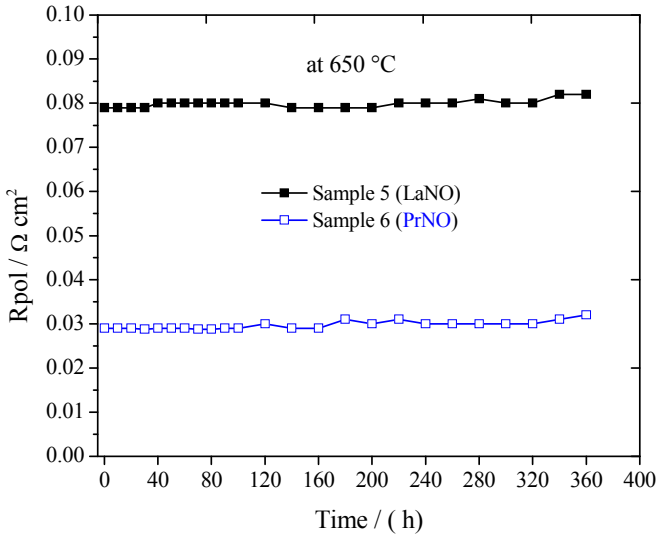

Fig. 10 Variation in the polarization resistance of samples 5 and 6 at 650 °C in OCV condition.

In summary, electrostatic spray deposition could be an effective method for commercial production of large-area electrodes for SOFCs with a series of advantages compared to the wet infiltration process, including easy industrial implementation, less preparation steps and low cost. Moreover, this method may be applicable to other electrochemical systems, such as solid electrolyzers, batteries, and supercapacitors.

4. Conclusions

This study demonstrates that the presence of a thin composite layer of CGO and LnNO in between electrolyte and the double layer LnNO cathodes deposited via SP and ESD procedures, respectively, is a very innovative route to improve significantly the electrochemical performance. Single phase of the prepared electrode crystallized in orthorhombic (Fmmm) has been confirmed by XRD. During the growth of the 3-D coral microstructure of LnNO on the top of thin compact CGO film, the precursor solution penetrates the compact CGO layer and leads to the formation of CGO and LnNO composite. In this work, cathodes containing CGO-LnNO composite sub layer displayed polarization resistances as low as 0.16 Ω cm^2 at 600 °C (0.04 Ω cm^2 at 700 °C) for LaNO and 0.04 Ω cm^2 at 600 °C (0.02 Ω cm^2 at 700 °C) for PrNO, which are among the best values reported so far for SOFC cathodes. The lowest values, found for these composite cathodes are due to the higher ionic conductivity of the composites, larger number of active points close to electrolyte, and larger contact area between CGO and LnNO which facilitate the

charge transfer from the cathode to the electrolyte. In addition, the R_{pol} values for both electrodes were found to be constant at 650 °C for 15 days, further proving their suitability to be used as SOFC cathode.

Acknowledgements

This work was performed within the framework of the Centre of Excellence of Multifunctional Architectured Materials "CEMAM" n° AN-10-LABX-44-01 funded by the "Investments for the Future" Program.

References:

1 A. Chroneos, D. Parfitt, J.A. Kilner and R.W. Grimes, *J. Mater. Chem.,* 2010, **20**, 266.

2 D. Pérez-Coll and A. Aguadero, *Fuel Cells*, 2011, **11**, 91.

3 V.V. Kharton, E.V. Tsipis, A.A. Yaremchenko and J.R. Frade, *Solid State Ionics*, 2004, **166**, 327.

4 F. Mauvy, J.M. Bassat, E. Boehm, P. Dordor and J.P. Loup, *Solid State Ionics*, 2003, **158**, 395.

5 F. Mauvy, E. Boehm, J.M. Bassat, J.C. Grenier and J. Fouletier, *Solid State Ionics*, 2007, **178**, 1200.

6 Q. Li, H. Zhao, L. Huo, L. Sun, X. Cheng and J-C. Grenier, *Electrochemistry Communications*, 2007, **9**, 1508.

7 A. Aguadero, J.A. Alonso, M.J. Escudero and L. Daza, *Solid State Ionics*, 2008, **179**, 393.

8 F. Mauvy, J.M. Bassat, E. Boehm, J.P. Manaud, P. Dordor and J.C. Grenier, *Solid State Ionics*, 2003, **158**, 17.

9 J.M. Bassat, P. Odier, A. Villesuzanne, C. Marin and M. Pouchard, *Solid State Ionics*, 2004, **167**, 341.

10 E. Boehm, J. Bassat, P. Dordor, F. Mauvy, J. Grenier and P. Stevens, *Solid State Ionics*, 2005, **176**, 2717.

11 C. Munnings, S.J. Skinner, G. Amow, P. Whitfield and I. Davidson, *Solid State Ionics*, 2005, **176**, 1895.

12 A. Tarancón, M. Burriel, J. Santiso, S. J. Skinner and J. A. Kilner, *J. Mater. Chem.*, 2010, **20**, 3799.

13 K. Yakal-Kremski, L. V. Mogni, A. Montenegro-Hernández, A. Caneiro and S.A. Barnett, *Journal of The Electrochemical Society*, 2014, **161**, F1366.

14 A. M. Daroukh, V.V. Vashook, H. Ullmann, F. Tietz and Arual Raj I., *Solid State Ionics*, 2003, 158, 141.

15 V.V. Kharton, A.P. Viskup, A.V. Kovalesvsky, E.N. Naumovich and F.M.B. Marques, *Solid State Ionics*, 2001, **143**, 337.

16 X. Dong, Z. Wu, X. Chang, W. Jin and N. Xu, *Ind. Eng. Chem. Res.*, 2007, **46**, 6910.

17 A.P. Khandale and S.S. Bhoga, *J. Power Sources*, 2010, **195**, 7974.

18 M.L. Fontaine, C. Laberty-Robert, F. Ansart and P. Tailhades, *J. Power Sources*, 2006, **156**, 33.

19 R. Sayers, M. Rieu, P. Lenormand, F. Ansart, J.A. Kilner and S.J. Skinner, *Solid State Ionics*, 2011, **192**, 531.

20 N. Hildenbrand, P. Nammensma, D.H.A. Blank, H.J.M. Bouwmeester and B.A. Boukamp, *J. Power Sources*, 2013, **238**, 442.

21 D. Marinha, L. Dessemond, J.S. Cronin, J.R. Wilson, S. A. Barnett and E. Djurado, *Chem. Mater.* 2011, **23**, 5340.

22 C. Ferchaud, J.C. Grenier,Y. Zhang-Steenwinkel, M.M.A. Van Tuel, F. P.F. Van Berkel and J.M. Bassat, *Journal of Power Sources*, 2011, **196**, 1872.

23 C. Jin and J. Liu, *J. Alloys Compd.,* 2009, **474**, 573.

24 S.J. Skinner a*nd G. Amow, Journal of Solid Sta**te** Chemistry*, 2007, **180**, 1977.

25 C. Tealdi, C. Ferrara, L. Malavasi, P Mustarelli, C Ritter and G. Chiodelli, *Physical Review B*, 2010, **82**, 174118.

26 S. Choi, S. Yoo, J.-Y. Shin and G. Kim, *J. Electrochem. Soc.*, 2011, **158**, B995.

27 C. Nicollet, A. Flura, V. Vibhu, A. Rougier, J-M. Bassat and J.C. Grenier, *Journal of Power Sources*, 2015, **294**, 473.

28 C. Nicollet, A. Flura, V. Vibhu, S. Fourcade, A. Rougier, J-M. Bassat and J.C. Grenier, *Journal of Solid State Electrochem*, 2016, 1.

29 V. Vibhu, A. Rougier, C. Nicollet, A. Flura, J.C. Grenier and J-M. Bassat, *Solid State Ionics*, 2015, **278**, 32.

30 Y. Huang, J. M. Vohs and R. J. Gorte, John Wiley & Sons, Inc., Hoboken, NJ, 2006; Vol. 179.

31 D. Ding, X. Li, S. Lai, K. Gerdes and M. Liu, *Energy Environ. Sci.* 2014, **7**, 552.

32 R. K. Sharma, M. Burriel, L. Dessemond, V. Martin, J.M. Bassat and Elisabeth Djurado, *Journal of Power Sources*, 2016, **316**, 17.

33 C.H. Chen, M.H.J. Emond, E.M. Kelder, B. Meester and J. Schoonman, *J. Aerosol. Sci.*, 1999, **30**, 959.

34 D. Marinha, L. Dessemond and E. Djurado, *Current Inorganic Chemistry*, 2013, **3**, 2.

35 J. Rodriguez-Carvajal, *Phys. B*, 1993, **192**, 55.

36 R. Neagu, D. Perednis, A. Princivalle and E. Djurado, *Solid State Ionics*, 2006, **177**, 1981.

37 C.H. Chen, E.M. Kelder, P.J.J.M. van der Put and J. Schoonman, *J. Mater. Chem.*, 1996, **6**, 765.

38 B.-H. Hwang, C.-L. Chang, C.-S. Hsu and C.-Y. Fu, *J. Phys. D: Appl. Phys.*, 2007, **40**, 3448.

39 J. Sar, O. Celikbilek, J. Villanova, L. Dessemond, C. L. Martin and E. Djurado, *Journal of the European Caramic Society*, 2015, **35**, 4497.

40 C. Fu, K. Sun, N. Zhang, X. Chen and D. Zhou, *Electrochim. Acta*, 2007, **52**, 4589.

41 S.B. Adler, *Solid State Ionics*, 2000, **135**, 603.

42 M.J. Escudero, A. Aguadero, J.A. Alonso and L. Daza, *J. Electroanal. Chem.*, 2007, **611**, 107.

43 T. Jacobsen, P.V. Hendriksen and S. Koch, Electrochimica Acta, 2008, **53**, 7500.

44 W.G. Bessler, Journal of the Electrochemical Society, 2006, **153**, A1492.

45 N. Hildenbrand, B. A. Boukamp, P. Nammensma and D.H.A. Blank, *Solid State Ionics*, 2011, **192** 12.

46 Z. Lou, J. Qiao, Y. Yan, J. Peng, Z. Wang and T. Jiang, *Int J Hydrogen Energy*, 2012, **37**, 11345.

47 S. Huang , Q. Lu, S. Feng , G. Li and C.Wang, *Adv. Energy Mater*, 2011, **1**, 1094.

48 H. Gu, H. Chen, L. Gao and L. Guo, *Electrochim Acta*, 2009, **54**, 7094.

49 L. Mogni, N. Grunbaum, F. Prado and A. Caneiro, *J. Electrochem. Soc.*, 2011, **158**, B202.

50 S. Pang, X. Jiang, X. Li, Q. Wang and Z. Su, *J. Power Sources*, 2012, **204**, 53.

51 B. Philippeau, F. Mauvy, C. Mazataud, S. Fourcade and J.C. Grenier, *Solid State Ionics*, 2013, **249-250**, 17.

Journal Name

ARTICLE

TOC

Triple layered $Ln_2NiO_{4+\delta}$ (Ln = La, Pr) cathodes, based on CGO-LnNO composite sub layer, lead to excellent electrical properties.